

Influence of transition elements (V, Zr and Mo) and cooling rate on the precipitation of dispersoids in Al-7Si-0.6Cu-0.35Mg foundry alloy

Dong Li¹, Kun Liu^{1,*}, and X-Grant Chen¹

¹Department of applied sciences, University of Quebec at Chicoutimi, Saguenay, (Quebec), Canada, G7H 2B1

Abstract. In the present work, individual/combined additions of transition elements (V, Zr and Mo) were introduced into Al-7Si-0.6Cu-0.35Mg foundry alloy at different cooling rates to study their influence on the precipitation behaviour of dispersoids. Results showed that both individual and combined additions of V, Zr, Mo lead to the formation of dispersoids but with different composition, morphology and number density during solution treatment. The addition of V produces the precipitation of both (Al,Si)₃M dispersoids and α -dispersoids, while the Zr addition promotes (Al,Si)₃M type dispersoids but inhibits the formation of α -Al(Mn,Fe)Si dispersoids. The addition of Mo effectively promotes α -Al(Mn,Mo,Fe)Si dispersoids and significantly reduces the dispersoid size and increase the number density of dispersoids. The combined addition of V, Zr and Mo produces the largest number of finer dispersoids among all five alloys studied, but the most dispersoids are (Al,Si)₃M. The (Al,Si)₃M dispersoids and α -dispersoids have the rod-like and block-like morphologies, respectively. High cooling rate can generally refine the dispersoids and increase their number density, while it also increases the proportion of (Al,Si)₃M dispersoids.

1 Introduction

Since commercially replacing cast iron with Al-Si foundry alloys in automotive engine applications, the weight of automobiles has been significantly reduced and consequently with better fuel efficiency. However, the mechanical properties of Al-Si alloys will significantly decrease with increasing temperature (above 200 °C) owing to the coarsening of conventional strengthening precipitates (mainly β' -Mg₂Si and θ' -Al₂Cu) [1, 2]. Therefore, how to improve the elevated-temperature properties of Al-Si foundry alloys is of primary importance for their sustainable development. On the other hand, the dispersion strengthening of thermally stable dispersoids has been proved to be one of the best strengthening ways for Al-Si alloys at elevated temperature [1, 3, 4].

According to the Lifshitz and Slyozov and Wagner theory, the ideal dispersed phase should have low interfacial energy (low lattice mismatch with matrix), low diffusivity and solubility limit, to prevent coarsening from bulk diffusion at the high temperature [5]. Since the transition elements like V, Zr and Mo have much lower diffusion rate ($4.85 \times 10^{-24} \text{ m}^2 \text{ s}^{-1}$, $1.20 \times 10^{-20} \text{ m}^2 \text{ s}^{-1}$ and $5.52 \times 10^{-23} \text{ m}^2 \text{ s}^{-1}$ at 400°C respectively) in the α -Al matrix than the common used dispersoid initiator of Mn ($6.24 \times 10^{-19} \text{ m}^2 \text{ s}^{-1}$ at 400 °C) [6], the dispersoids containing these elements are expected to have better coarsening resistance.

The strengthening by nanoscale L1₂ metastable Al₃M type precipitates that can maintain their coherency with the matrix at elevated temperatures is often applied in aluminum wrought alloys [5-7]. However, the existence of Al₃Zr (L1₂) in Al-Si foundry alloys with high Si level (>3 wt.%) has rarely been observed [8-12]. It is widely accepted that the addition of Zr in Al-Si alloys leads to the formation of equilibrium rod-shaped (Al,Si)₃Zr (D0₂₃) dispersoids [13, 14].

V is an extraordinarily sluggish diffuser in the α -Al matrix. Although Al₃V is not considered to be in equilibrium with α -Al [6], the Al₃V_{1-x}M_x trialuminide has low lattice mismatch with the α -Al matrix and thereby potentially being thermally stable [15]. It is reported that when Zr, V, and Ti were simultaneously added into Al7Si1Cu0.5Mg alloy, the rod-shaped Zr,V,Ti-containing dispersoids precipitated [12]. V is also reported to be able to promote the precipitation of α -Al(Mn,V,Fe)Si dispersoids by substituting Mn of α -Al(Mn, Fe)Si [16, 17]. Therefore, it is expected that (Al,Si)₃M and α -Al(Mn,Fe)Si dispersoids with modification of V are thermally stable.

It is recently discovered that Mo is a supreme dispersoid former in both aluminum foundry and wrought alloys [1, 3, 4, 18]. The combination of Mn and Mo can lead to a uniform distribution of partially coherent α -Al(Mn,Mo,Fe)Si dispersoids and reduce the dispersoid free zone, because of their opposite solid-liquid partition coefficient during solidification [18].

* Corresponding author: kun.liu@uqac.ca

High cooling rate can refine the as-cast microstructure but increase the area fraction of eutectics in Al-Mg-Si alloys due to the greater segregation effect of the solute atoms [19]. It can also reduce the size of intermetallic particles in Al-Si-Cu-Mg casting alloys [20]. High cooling rate with fine dendrite arm spacing generally results in high strengths and elongation as well as improved fatigue properties [20, 21].

As reviewed above, although several works have been done to study the effect of individual transition element on the microstructures and properties, the influence of combined V, Zr and Mo as well as the cooling rate on the dispersoids precipitation in Al-Si foundry alloys has not been systematically investigated. Therefore, the aim of the present work is to investigate the effects of individual and combined additions of V, Zr and Mo and cooling rate on cast microstructure and the precipitation behavior of dispersoids in Al-7Si-0.6Cu-0.35Mg alloys.

2 Experimental procedure

Five Al-Si-Cu-Mg foundry alloys with different V, Zr and Mo contents were prepared with commercial pure Al (99.6%), pure Mg (99.9%), Al-50%Si, Al-25%Mn, Al-5%Ti-1%B, Al-50%Cu, Al-10%Sr, Al-5%V, Al-15%Zr and Al-10%Mo master alloys. Their chemical compositions analyzed by an optical emission spectrometer are shown in Table 1. For each alloy, approximately 3.5 kg of materials were melted in a clay-graphite crucible using an electric resistance furnace. The liquid metal was maintained at approximately 750 °C for 30 min and then degassed for 15 min with high purity Ar. All five batches were grain-refined by adding the Al-5%Ti-1%B master alloy and modified by the addition of Al-10%Sr master alloy. The liquid metal was poured into the permanent mold preheated at 250 °C. In the present work, two different permanent molds were used to test the effect of the cooling rate on the evolution of microstructure; one is permanent steel mold with a low cooling rate (~2°C/s) and the other is permanent copper mold with a high cooling rate (~10 °C/s). The sample from the steel mold was “Y” block shape with a dimension of 80mm×40mm×30mm, which was designated as “Y” while the sample from the copper mold was the thin plate with a dimension of 100mm×80mm×4.5mm and designated as “S” in the present work. After casting, all samples were subjected a two-step solution treatment (500°C/2h + 520°C/2~12h) to evaluate the formation of dispersoids according to the literatures [22, 23].

Table 1. Chemical composition of experimental alloys (wt.%)

No.	Si	Fe	Mg	Mn	Ti	Cu	Sr	V	Zr	Mo	Al
0	7.3	0.13	0.36	0.18	0.19	0.61	0.01	-	-	-	Bal.
1	7.4	0.15	0.35	0.20	0.20	0.60	0.01	0.28	-	-	Bal.
2	7.2	0.13	0.35	0.18	0.19	0.59	0.01	-	0.23	-	Bal.
3	7.4	0.14	0.35	0.20	0.19	0.60	0.01	-	-	0.31	Bal.
4	6.8	0.12	0.33	0.20	0.19	0.60	0.01	0.20	0.20	0.28	Bal.

To investigate the evolution of microstructures, such as the formation of intermetallics and dispersoids, an optical microscope (OM), a scanning electron microscope (SEM) equipped with energy dispersive spectroscopy (EDS) and electron backscatter diffraction (EBSD) and a transmission electron microscope (TEM) operated at 200 kV were employed.

In addition, Vickers microhardness were measured to evaluate the room-temperature properties. The tests were conducted at room temperature by NG-1000 CCD micro-hardness test machine with a 10g load and a 20s dwelling time. 10 measurements were performed in the α -Al matrix to calculate the average hardness value for each sample. Electrical conductivity was measured by Sigmascope SMP10 electrical conductivity test device at room temperature, with 10 measurements for each sample.

3 Results and Discussion

3.1 As-cast and solutionized microstructures

In the present work, the as-cast microstructures of experimental alloys are observed to be composed of dendritic α -Al, eutectic silicon and various intermetallic phases, which exhibit a variety of types and morphologies and highly depend on the addition of transition elements. The high cooling rate (S-samples) produced finer microstructures including the second arm spacing (SDAS), Si particles and intermetallics, compared to the low cooling rate (Y-samples). The as-cast S samples have the average SDAS of 20 μ m, while the average SDAS of Y samples is 35 μ m. As an example, the typical as-cast microstructures of #4 alloy under two cooling rates are exemplarily given in Fig. 1, which displays the various intermetallics formed due to the combined addition of transition elements as well as the finer microstructures in S-sample (Fig. 1b).

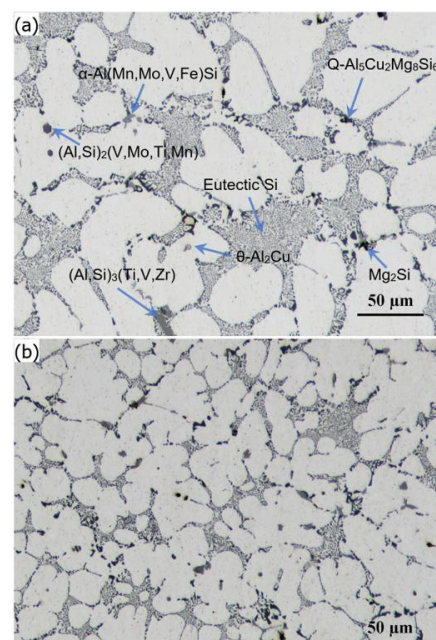


Fig. 1. As-cast microstructure of #4 alloy of (a) Y-sample and (b) S-sample.

The #0 base alloy has a major α -Al(Mn,Fe)Si intermetallic phase and a trace $(Al,Si)_3Ti$ intermetallic due to presence of Ti by the grain refinement addition. In V-added #1 alloy, in addition to the major α -Al(Mn,V,Fe)Si intermetallic, a $(Al,Si)_2(V,Ti,Mn)$ phase were found as suggested by [17, 24] with some Si substituted by Al and some V substituted by Ti and Mn on the basis of Si_2V phases because of their similar atomic radius [25]. Similarly, in Mo-added #3 alloy, some (Mo,Si)-rich $(Al,Si)_2(Mo,Ti,Mn)$ intermetallic particles were also found derived from $Mo(Al,Si)_2$ phase [26, 27]. In #4 alloy with the combined addition of V, Zr and Mo, three main intermetallic phases with complicate chemical composition were found, which are α -Al(Mn,Mo,V,Fe)Si phase, plate-like $(Al,Si)_3(Ti,V,Zr)$ and hexagonal $(Al,Si)_2(V,Mo,Ti,Mn)$. It should be mentioned that all five alloys contain Mg_2Si , and two Cu-containing θ - Al_2Cu and Q - $Al_5Cu_2Mg_8Si_6$ phases due to the presence of Mg, Si and Cu in experimental alloys. The details of various intermetallic phases found and identified in as-cast microstructures of five alloys are summarized in Table 2.

Table 2. Intermetallic phases in the as-cast microstructure of different alloys

Alloys	Intermetallic phases
#0	α -Al(Mn,Fe)Si, $(Al,Si)_3Ti$
#1	α -Al(Mn,V,Fe)Si, $(Al,Si)_3(Ti,V)$, $(Al,Si)_2(V,Ti,Mn)$
#2	α -Al(Mn,Fe)Si, $(Al,Si)_3(Ti,Zr)$
#3	α -Al(Mn,Mo,Fe)Si, $(Al,Si)_3Ti$, $(Al,Si)_2(Mo,Ti,Mn)$
#4	α -Al(Mn,Mo,V,Fe)Si, $(Al,Si)_3(Ti,V,Zr)$, $(Al,Si)_2(V,Mo,Ti,Mn)$

During two-step solution treatment, the eutectic Si particles were spheroidized, while all three low melting point Mg/Cu-containing intermetallic phases, including Mg_2Si , θ - Al_2Cu and Q - $Al_5Cu_2Mg_8Si_6$, were fully dissolved into the α -Al matrix. In general, the Fe/Ti/V/Zr/Mo-containing intermetallic phases (in the left column of Table 2) were the high melting point phases. They may be fragmented and partially dissolved during solution treatment at 520 °C but most of them remain in the microstructure after solution treatment. Fig. 2 gives an example of as-solutionized microstructure of the #4-Y sample, in which the α -Al(Mn,Mo,V,Fe)Si, $(Al,Si)_3(Ti,V,Zr)$ and $(Al,Si)_2(V,Mo,Ti,Mn)$ phases formed during solidification were still observed after solution treatment.

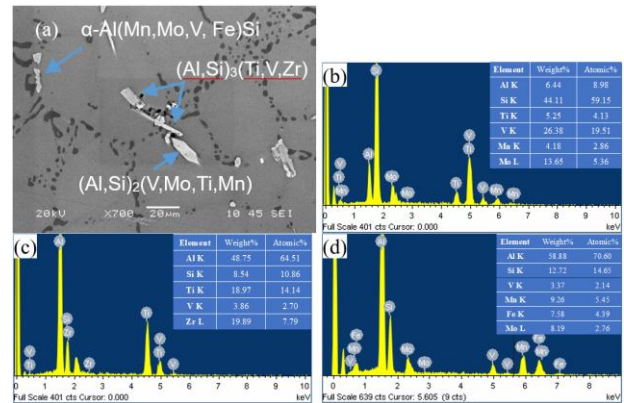


Fig. 2. SEM secondary electron image of the #4-Y sample after 520 °C solution treatment for 4 h (a) with EDS analysis results of intermetallics: (b) $(Al,Si)_2(V,Mo,Ti,Mn)$; (c) $(Al,Si)_3(Ti,V,Zr)$; (d) α -Al(Mn,Mo,V,Fe)Si.

The total volume fractions of remaining intermetallic phases after solution treatment in different alloys were measured to evaluate the effects of different solute elements and cooling rate on their formation, and results are shown in Fig. 3. It can be found that the #0 base alloy has the lowest volume fractions of intermetallics at both cooling rates. With the addition of transition elements, the volume fractions of intermetallics increase, while the high cooling rate reduces the formation of intermetallics and more transition elements can be retained in the α -Al matrix. It is evident that the #4 alloy with combined addition possesses the highest volume fraction of intermetallics, which has more than doubled intermetallic fraction relative to the base alloy. The Zr-added #2 alloy has the second highest volume fraction of intermetallics among all alloys but the largest intermetallics fraction among three individual transition element added alloys (#1 to #3) due to the low solute ability of Zr in Al.

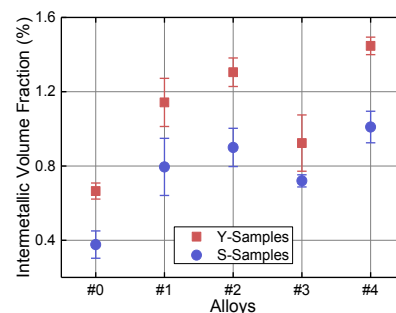


Fig. 3. Volume fraction of remained intermetallic phases after 520°C/4h solution treatment in various alloys

3.2 Formation of dispersoids during solution treatment

In Al-Si foundry alloys, the dispersoids usually form during solution treatment [1, 4, 18, 23]. To monitor the precipitation of dispersoids during solution treatment and to compare the hardening effect of the transition elements, Vickers microhardness (HV) and electrical conductivity (EC) as a function of holding time were measured and the results are shown in Fig. 4.

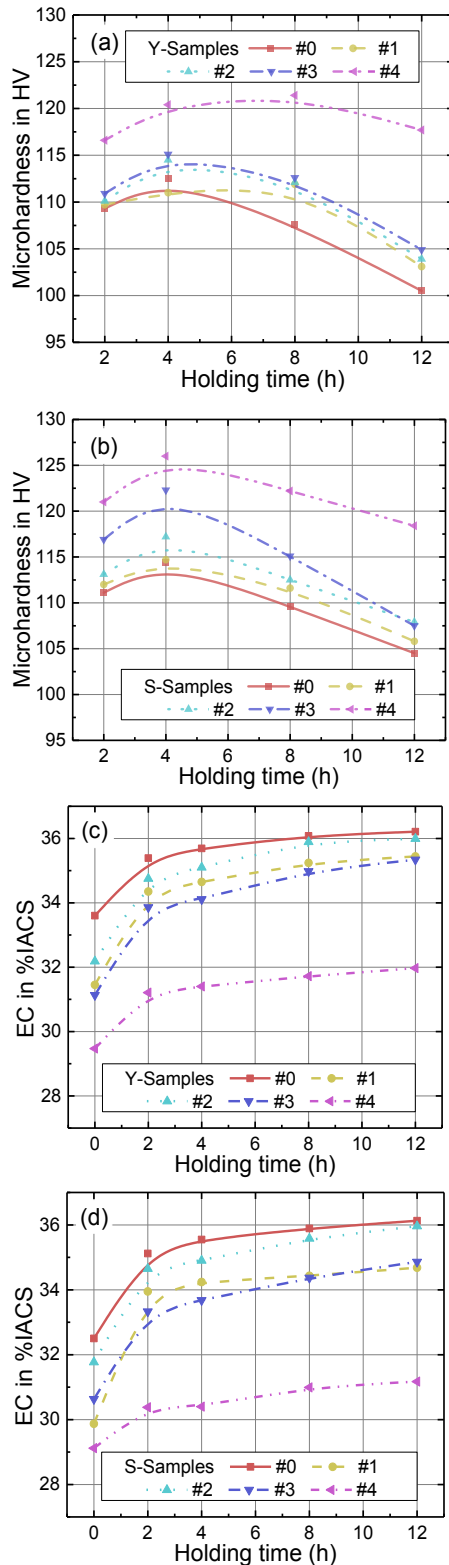


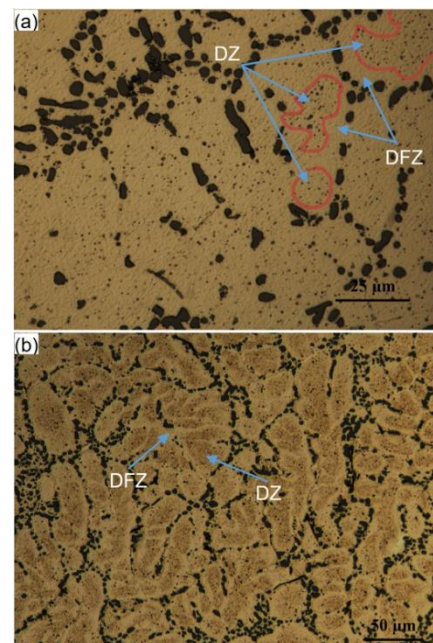
Fig. 4. Vickers microhardness (a, b) and electrical conductivity (c, d) as a function of holding time during solution treatment at 520 °C in different alloys

Except of the consumption in the intermetallic phases, all dispersoid-forming alloy elements (Mn, Fe, Si, Zr, V and Mo) are supersaturated in the as-cast microstructure. During solution treatment and with increasing holding time, both microhardness and EC gradually increase, indicating the dispersoids precipitate from the supersaturated aluminum matrix. At both

cooling rates, the peak microhardness is reached after 4 h holding time (Fig. 4a-b), while the EC also approaches the maximum value (Fig. 4c-d), suggesting that the dispersoids are fully precipitated after 520°C/4h; thereby the 520°C/4h solution treatment is chosen for further metallographic investigation of the dispersoids. With prolonged holding time after 4 h, the values of microhardness of all five alloys exhibit a decreasing tendency, while the EC values reach a plateau, which is most likely attributed to that the dispersoids start to coarsen with prolonged holding time at 520 °C.

The microhardness differences between different alloys are mainly ascribed to the amount of precipitated dispersoids and their strengthening effect. As shown in Fig. 4a-b, the #4 alloy with combined addition of V, Zr and Mo has the highest microhardness among all of the alloys at any given holding time. The Mo-added #3 alloy has an obvious improvement, showing the second highest microhardness. The #1 and #2 alloys show only a slight improvement compared to the #0 alloy. In addition, the high cooling rate (S-samples) always has the higher microhardness compared to the low cooling rate (Y-samples) for each alloy, suggesting the higher amount of precipitated dispersoids due to the higher supersaturated level at the high cooling rate condition.

The dispersoids usually precipitate within dendrite cells (the dispersoid zone (DZ) in the intradendritic region). In the outside of the dispersoid zone, it forms the dispersoid free zone (DFZ), which locates closely to the dendrite boundaries and intermetallic particles due to the depleted alloying solutes at the area. Fig. 5 shows optical images giving an overview of the distribution of the dispersoid zones and dispersoid free zones after solution treatment in the #0, #1 and #3 alloys as examples. All of the samples are etched with 0.5% HF for 90 s in order to reveal the DZs and DFZs clearly. It can be found the volume of DZ is lower but with higher DFZ in #0 compared with #1 and #3 alloys while #3 has the maximum volume of DZ.



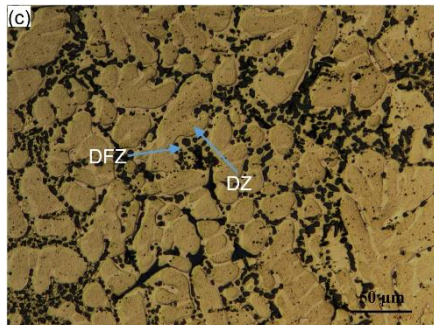


Fig. 5. Dispersoid zone (DZ) and dispersoid free zone (DFZ) formed during solution treatment (520°C/4h) (etched with 0.5%HF for 90s): (a) #0-S; (b) #1-S; (c) #3-S.

The measured area fractions of DZs in different alloys are shown in Table 3. Based on the measurements, it is clear to see that the cooling rates have limited influence on the fraction of DZ, while the added transition elements have strong effects on it, which can be related to the inverse of their partition coefficients (k_0 (Mn, Fe and Si) < 1 while k_0 (Ti, V, Zr and Mo) > 1 [6, 17, 18]). Therefore, the formation of DZ was increased with transition elements. The maximum DZ fraction was found in #3 alloy, around 73% with both molds, indicating that Mo is a strong DFZ eliminating element for Al-Si-Cu-Mg foundry alloys. The #1, #2 and #4 alloys have similar DZ fractions which are smaller than that of #3 alloy, because of their relatively larger DFZs around the dendrite boundaries, as we can see in Fig. 4b-c. However, they absolutely have larger DZs compared to #0 alloy whose DZs are even hard to be identified, as shown in Fig. 5a.

Table 3. Area fractions of DZs in solutionized alloys

DZ Fraction (%)	#0	#1	#2	#3	#4
Y-Samples	41±5	64±6	64±8	74±5	66±7
S-Samples	44±4	62±7	65±6	73±3	68±7

To study the details of the dispersoids (type, morphology, size and number density), TEM investigation is carried out for each alloy condition, and the distribution of dispersoids in DZ of experimental alloys is shown in Fig. 6.

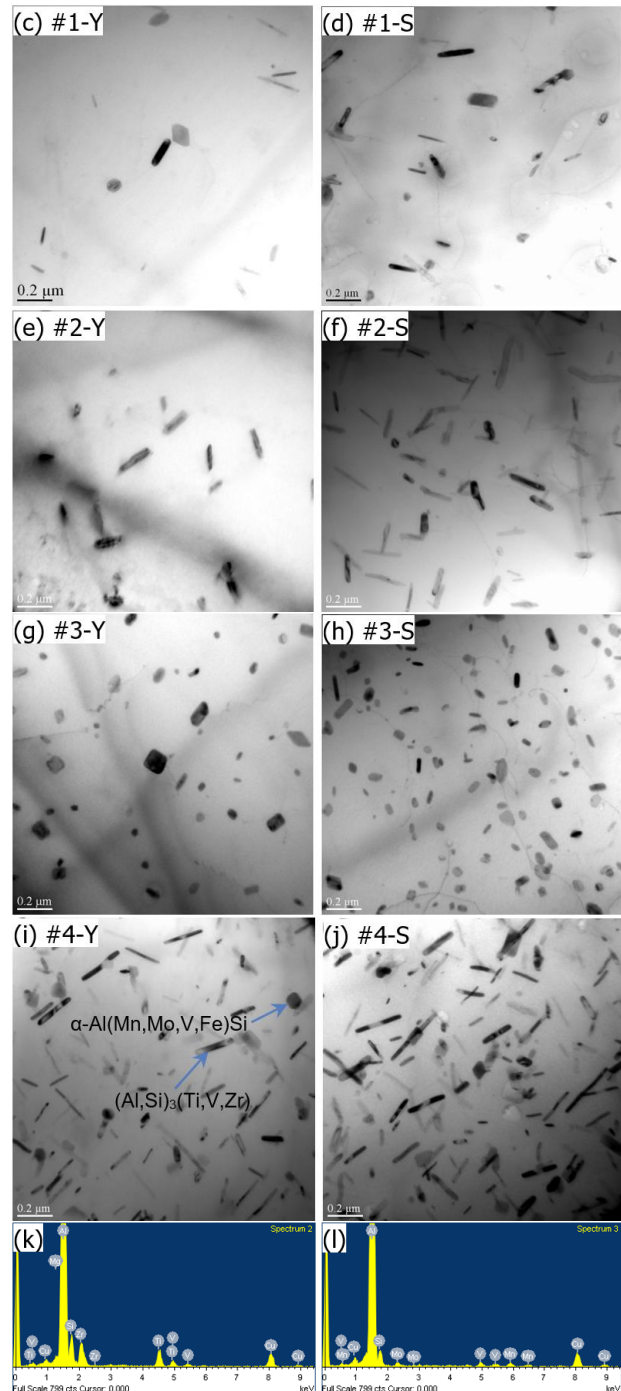
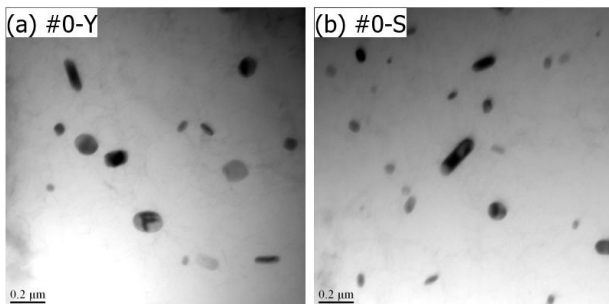


Fig. 6. TEM images revealing the dispersoids in all alloy conditions with Y-Samples and S-Samples (a-j); TEM-EDS results of typical $(Al,Si)_3(Ti,V,Zr)$ and $\alpha-Al(Mn,Mo,V,Fe)Si$ dispersoids (k-l).

To help the identification of the dispersoids, TEM-EDS was used to analyze the chemical compositions of different dispersoid types. In general, the dispersoids found under TEM can be divided into two groups: $\alpha-Al(Mn,Fe)Si$ type dispersoids with block-like morphology and $(Al,Si)_3M$ type dispersoids with rod/plate-like morphology and their distribution in experimental alloys are summarized in Table 4. The morphology difference between these two kinds of dispersoids may be explained by their respective cubic and $D0_{22}/D0_{23}$ tetragonal crystal structures [13, 18, 28, 29]. In addition, the overall equivalent diameter and

number densities of the dispersoids were quantitatively analyzed based on the image analysis on TEM images, with ratios of the 2 types of dispersoids empirically estimated based on the TEM-EDS results in each alloy condition, as showed in Fig. 7.

Table 4. Dispersoids observed in TEM

Alloys	Dispersoids
#0	α -Al(Mn,Fe)Si
#1	α -Al(Mn,V,Fe)Si, (Al,Si) ₃ (Ti,V)
#2	(Al,Si) ₃ (Ti,Zr)*, α -Al(Mn,Fe)Si
#3	α -Al(Mn,Mo,Fe)Si
#4	(Al,Si) ₃ (Ti,V,Zr)*, α -Al(Mn,Mo,V,Fe)Si,

* Dominant dispersoids

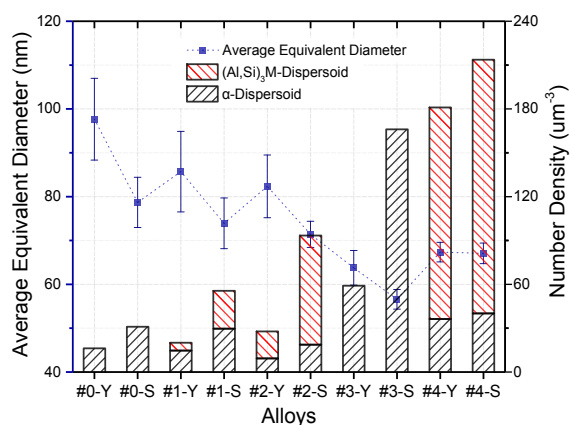


Fig. 7. Average dispersoid equivalent diameters and number densities in different alloys and molds

In the #0 base alloys, a number of block-like dispersoids occurred (Fig. 6a-b), which are identified as α -Al(Mn,Fe)Si, due to the presence of Mn in the base alloy [1, 19, 24]. However, the base alloy has the largest average dispersoid diameter (98 nm in Y-samples and 79 nm in S-samples) and the lowest number density compared with other alloys.

In the V-added #1 alloy, the number density of block-like α -dispersoids seems to be similar with base alloy but with smaller size. In addition, the rod-like (Al,Si)₃(Ti,V) dispersoids also formed (Fig. 6c-d). The average dispersoid diameters are 86 nm in Y-samples and 74 nm in S-samples, which is moderately decreased relative to the #0 alloy. At the high cooling rate (S-samples), the proportion of (Al,Si)₃(Ti,V) dispersoids is higher than Y sample, which is even similar to α -dispersoids.

In the Zr-added #2 alloy, a number of (Al,Si)₃(Ti,Zr) with rod-like morphology formed instead of α -dispersoids (Fig. 6e-f). Since Zr has a very limited solubility in Al, 0.083 at.% of maximum equilibrium solid solubility and 0.0005 at.% at 400 °C [6], the number density of (Al,Si)₃(Ti,Zr) dispersoids formed in the #2 alloy is relatively low at the lower cooling rate. However, the formation of (Al,Si)₃(Ti,Zr) dispersoids is strongly promoted (Fig. 6f) at higher cooling rate (S-samples) and become the majority of dispersoids with a relatively high number density (Fig. 7) but the formation of α -Al(Mn,Fe)Si dispersoid seems to be inhibited. The

average dispersoids diameter are 82 nm in Y-samples and 71 nm in S-samples, which is slightly smaller than #1 alloy.

The addition of Mo in the #3 alloy effectively promoted the formation of α -Al(Mn,Mo,Fe)Si dispersoids with block-like morphology, which are the only dispersoids found in the microstructure (Fig. 6g-h). The alloy has the lowest dispersoid diameter (65 nm in Y-samples and 58 nm in S-samples) among all five alloys. In addition, the number densities of dispersoids in the #3 alloy increase significantly compared to the #0, #1 and #2 alloys. Besides, the ideal interaction of Mo and Mn also lead to the largest DZ fraction as mentioned above.

The synergistic effect of the combined addition of V, Zr and Mo in the #4 alloy is quite complicated. Obviously, the alloy produces the largest number of fine dispersoids among all five alloys (Fig. 6i-j). The average dispersoid size is around 67 nm in both Y- and S-samples, which is remarkably finer than the #0, #1 and #2 alloys but slightly coarser than the #3 alloy. However, it has the highest number densities among all five alloys (Fig. 7). Probable owing to the combined effect of V and Zr, most of the dispersoids in the #4 alloys are rod-shape (Al,Si)₃(Ti,V,Zr), which are preferred to precipitate around the center of dendrite cells and the promotion from Mo appears to be affected. As a result, the DZ fraction in #4 alloy is not as large as that in #3 alloy.

Regarding the number density of the dispersoids, the individual addition of V or Zr in the #1 and #2 alloys has a limited increase compared to the base alloy. The Mo addition and the combined addition of V, Zr and Mo have a large impact on the number density and these two alloys possess much higher number densities at both cooling rates than the #0, #1 and #2 alloys (Fig. 7). Owing to its highest number density of fine dispersoids, the combined addition of V, Zr and Mo induces the largest hardening effect among all five alloys. For individual additions of V, Zr or Mo, the sequence of hardening effect due to dispersoid strengthening is Mo > Zr > V (Fig. 4a-b).

The high cooling rate increases the number density and decreases the size of dispersoids in all 5 alloys. On the other hand, with the additions of V and Zr in #1, #2 and #4 alloys, it is also worthy to notice that the high cooling rate usually leads to a higher portion of rod-like (Al,Si)₃M type dispersoids owing to the increase of V, Zr and Ti content in solid solution.

The authors would like to acknowledge the financial support of the Natural Sciences and Engineering Research Council of Canada (NSERC) and Rio Tinto Aluminum through the Research Chair in the Metallurgy of Aluminum Transformation at University of Quebec in Chicoutimi.

4 Conclusion

- 1) The addition of V in Al-7Si-0.6Cu-0.35Mg foundry alloy mainly produces the precipitation of

(Al,Si)₃(Ti,V) dispersoids but has limited influence on α -Al(Mn,V,Fe)Si dispersoids during the solution treatment; while the addition of Zr greatly increase the volume of (Al,Si)₃(Ti,Zr) dispersoids but inhibits the formation of α -Al(Mn,Fe)Si dispersoids. The individual addition of V or Zr fairly reduces the dispersoid size and moderately increases the number density of the dispersoids relative to the base alloy.

- 2) The addition of Mo effectively promotes the precipitation of α -Al(Mn,Mo,Fe)Si dispersoids and significantly reduces the dispersoid size, exhibiting the lowest dispersoid diameter among all five alloys studied. In addition, the number density of dispersoids in the alloy increases significantly compared to the V-added or Zr-added alloys.
- 3) The combined addition of V, Zr and Mo produces the largest number of fine dispersoids among all five alloys studied. Owing to the combined effect of V and Zr, most of the dispersoids in the alloys are rod-like (Al,Si)₃(Ti,V,Zr). The alloy shows considerably higher hardening effect than all other alloys owing to its highest dispersoid strengthening contribution. For individual additions of V, Zr or Mo, the sequence of hardening effect due to dispersoid strengthening is Mo > Zr > V.
- 4) The high cooling rate not only decrease the SDAS and fraction of intermetallics in as-cast microstructure, but also refines the dispersoid size and increases the number density of dispersoids in all of the alloys studied during the solution treatment. In addition, it increases the proportion of (Al,Si)₃M type dispersoids in the microstructure of V or Zr added alloys.

References

1. A. R. Farkoosh, X. Grant Chen, M. Pekguleryuz. *Mater. Sci. Eng., A*. **620**, 181-189 (2015).
2. M. Javidani, D. Larouche. *Int. Mater. Rev.* **59**, 132-158 (2014).
3. K. Liu, H. Ma, X. G. Chen. *J. Alloys Compd.* **694**, 354-365 (2017).
4. L. Jin, K. Liu, X. G. Chen. *J. Mater. Eng. Perform.* (2020).
5. M. Zedalis, M. Fine. *Metall. Trans. A*. **17**, 2187-2198 (1986).
6. K. E. Knippling. Development of a nanoscale precipitation-strengthened creep-resistant aluminum alloy containing trialuminide precipitates. DOCTOR OF PHILOSOPHY, Northwestern University, 2006.
7. D. Tsivoulas, J. Robson. *Acta Mater.* **93**, 73-86 (2015).
8. P. Sepehrband, R. Mahmudi, F. Khomamizadeh. *Scripta Mater.* **52**, 253-257 (2005).
9. R. Mahmudi, P. Sepehrband, H. Ghasemi. *Mater. Lett.* **60**, 2606-2610 (2006).
10. H. A. Elhadari, H. A. Patel, D. L. Chen, W. Kasprzak. *Mater. Sci. Eng., A*. **528**, 8128-8138 (2011).
11. B. Baradarani, R. Raiszadeh. *Mater. Des.* **32**, 935-940 (2011).
12. W. Kasprzak, B. S. Amirkhiz, M. Niewczas. *J. Alloys Compd.* **595**, 67-79 (2014).
13. T. Gao, A. Ceguerra, A. Breen, X. Liu, Y. Wu, S. Ringer. *J. Alloys Compd.* **674**, 125-130 (2016).
14. M. Rahimian, S. Amirkhanlou, P. Blake, S. Ji. *Mater. Sci. Eng., A*. **721**, 328-338 (2018).
15. K. E. Knippling. *Microsc. Microanal.* **21**, 359-360 (2015).
16. Y. Wu, H. Liao, K. Zhou. *Mater. Sci. Eng., A*. **602**, 41-48 (2014).
17. J. Rakhmonov, G. Timelli, A. Fabrizi, F. Bonollo. *International Journal of Materials Research.* **109**, 1099-1112 (2018).
18. A. R. Farkoosh, X. Grant Chen, M. Pekguleryuz. *Mater. Sci. Eng., A*. **627**, 127-138 (2015).
19. W. Fei, S. Kang. *J. Mater. Sci. Lett.* **14**, 1795-1797 (1995).
20. L. Ceschini, A. Morri, S. Toschi, S. Seifeddine, S. Messieri. *Mater. Sci. Forum.* **884**, 81-92 (2017).
21. B. Zhu, P. Leisner, S. Seifeddine, A. E. W. Jarfors. *Surf. Interface Anal.* **48**, 861-869 (2016).
22. A. Samuel, F. Samuel. *Journal of Materials Science.* **27**, 6533-6563 (1992).
23. S. Chen, K. Liu, X. G. Chen. *J. Mater. Res.* **34**, 3071-3081 (2019).
24. J. Rakhmonov, G. Timelli, F. Bonollo. *Mater. Charact.* **128**, 100-108 (2017).
25. B. Huber, H. S. Effenberger, K. W. Richter. *Intermetallics.* **18**, 606-615 (2010).
26. C. Guo, C. Li, P. J. Masset, Z. Du. *Calphad.* **36**, 100-109 (2012).
27. C. E. Ramberg, W. L. Worrell. *J. Am. Ceram. Soc.* **83**, 946-948 (2000).
28. S. Yamaguchi. *Keikinzoku.* **38**, 228-238 (1988).
29. Y. Li, A. Muggerud, A. Olsen, T. Furu. *Acta Mater.* **60**, 1004-1014 (2012).